# Discrete vortices on spatially nonuniform two-dimensional electric networks

Victor P. Ruban*

*Landau Institute for Theoretical Physics, RAS, Chernogolovka, Moscow Region, 142432 Russia*

(Received 18 October 2019; revised 12 March 2020; accepted 19 June 2020; published 7 July 2020)

Two-dimensional arrays of nonlinear electric oscillators are considered theoretically where nearest neighbors are coupled by relatively small constant but nonequal capacitors. The dynamics is approximately reduced to a weakly dissipative defocusing discrete nonlinear Schrödinger equation with translationally noninvariant linear dispersive coefficients. Behavior of quantized discrete vortices in such systems is shown to depend strongly on the spatial profile of the internode coupling as well as on the ratio between time-increasing healing length and lattice spacings. In particular, vortex clusters can be stably trapped for some initial period of time by a circular barrier in the coupling profile, but then, due to gradual dissipative broadening of vortex cores, they lose stability and suddenly start to move.

DOI: 10.1103/PhysRevE.102.012204

## I. INTRODUCTION

Nonlinear complex wave fields are known to support quantized vortices in two and three spatial dimensions [1–8]. Vortices have also been studied in discrete systems (on lattices; see, e.g., Refs. [9–16] and citations therein). As far as weakly dissipative lattice dynamics is considered, among the most popular mathematical models are modifications of a discrete nonlinear Schrödinger equation (DNLSE) [9–25]. They arise in various scientific contexts (but mostly in nonlinear optics [13,15] and in physics of nonlinear metamaterials [16]), where we have nearly identical oscillators with their normal complex variables $a_n(t) = A_n(t)\exp(-i\omega_0 t)$ and with nonlinear frequency shifts $g|A_n|^2 \ll \omega_0$. The simplest form of the DNLSE is

$$i(\dot{A}_n + \gamma\omega_0 A_n) = g|A_n|^2 A_n - \frac{1}{2}\sum_{n'} c_{n,n'} A_{n'}, \qquad (1)$$

where the overdot means a time derivative. A linear damping rate $\gamma\omega_0$ takes into account dissipative effects with small $\gamma = 1/Q \ll 1$ being an inverse quality factor. Oscillators are weakly coupled by (real) coefficients $c_{n,n'} = c_{n',n} \ll \omega_0$ (if coupling strength and/or nonlinearity level are not weak, then, more complicated forms of the DNLSE appear, including nonlinearities in coupling terms [13,15]). In many interesting cases, multi-index $n$ is a node $\mathbf{n} = (n_1, \ldots, n_d)$ of a simple regular lattice in one, two, or three spatial dimensions ($d = 1$, $d = 2$, and $d = 3$, respectively). Besides electromagnetic artificially created structures [16], the DNLSE has been successfully applied in nonlinear optics where it describes a stationary regime of light propagation in waveguide arrays [13] [one-dimensional (1D) and two-dimensional (2D) cases with time variable $t$ replaced by propagation coordinate $z$].

The coupling coefficients $c_{\mathbf{n},\mathbf{n}'}$ are often considered as translationally invariant on the lattice and taking place between a few near neighbors. If they have a definite sign, then, in the long-scale quasicontinuous limit, we have either a defocusing regime (when $gc > 0$), or a focusing one (when $gc < 0$). Accordingly, different nonlinear coherent wave structures can take place in each case. In particular, in the most well-studied focusing regime, there are highly localized discrete solitons and discrete vortex solitons (see Refs. [9–13]), and references therein). In the defocusing regime, there are dark solitons, and besides that, discrete analogs of superfluid quantized vortices can be excited and interact with each other over long distances.

In this paper, we consider discrete vortices but in somewhat more complicated arrangements where coupling coefficients are not translationally invariant $c_{\mathbf{n}+\mathbf{l},\mathbf{n}'+\mathbf{l}} \neq c_{\mathbf{n},\mathbf{n}'}$, and the corresponding terms contain differences $(A_n - A_{n'})$ instead of $(-A_{n'})$,

$$i(\dot{A}_n + \gamma\omega_0 A_n) = g|A_n|^2 A_n + \frac{1}{2}\sum_{n'} c_{n,n'}(A_n - A_{n'}). \qquad (2)$$

In general, Eqs. (1) and (2) are not equivalent. The exception is for infinite and uniform lattices where they are related to each other by a simple gauge transformation.

It is important that Eq. (2) with any coefficients $c_{n,n'}$ admits a class of spatially uniform solutions,

$$A_n = A_0\exp[-\gamma\omega_0 t - ig|A_0|^2(1 - e^{-2\gamma\omega_0 t})/(2\gamma\omega_0)]. \qquad (3)$$

However, spatial nonuniformity of couplings should strongly affect vortex dynamics on the above background since vortices are known to have highly delocalized phase gradients, even if the amplitude variation (vortex core) is localized. Continuous quantized vortices on spatially nonuniform backgrounds have been extensively studied in application to trapped Bose-Einstein condensates where nonuniformity is introduced by external potential (see, e.g., Refs. [5–8,26–49] and citations therein). Effects of dispersive nonuniformity are still waiting for studying. Therefore, the first goal of this paper is to investigate such effects for vortices on discrete lattices within model (2). For simplicity, we consider below a square lattice and interactions between the nearest neighbors

*ruban@itp.ac.ru

 

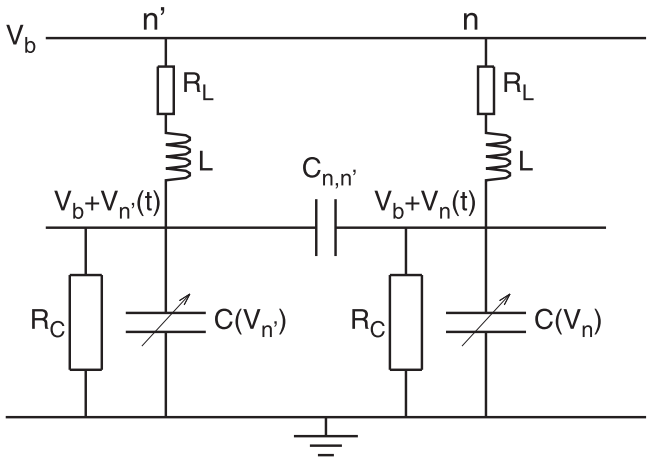


FIG. 1. Schematic representation of coupled oscillators. Only a fragment of the whole network is shown (two cells and coupling between them).

in the form

$$c_{\mathbf{n},\mathbf{n}'} = f(h[\mathbf{n}+\mathbf{n}']/2), \tag{4}$$

where $h \ll 1$ is a lattice spacing and $f(x, y)$ is a sign-definite function varying on scales $(\Delta x; \Delta y) \sim 1$.

Equation (2) with nonuniform couplings has been introduced recently in a formal manner as a three-dimensional (3D) discrete system supporting long-lived vortex knots [25]. But no physical prototype was indicated there. In the present paper, as a possible physical implementation approximately corresponding to this equation, we theoretically suggest and analyze a specially designed electric circuit network. Implementation of discrete nonlinear dynamic systems in the form of 1D and 2D electric networks has a long and rich history [50–64], including even experimental simulations of the integrable Toda chain [50–53]. Major attention has been devoted to modulationally unstable systems. Here, we consider a network possessing stable solutions (3). We adopt a scheme consisting of nonlinear oscillator circuits coupled by relatively small nonequal capacitors as shown in Fig. 1. It will be derived below that nonlinear constant $g$ and coupling coefficients $c_{\mathbf{n},\mathbf{n}'}$ appear both negative in this case, so the corresponding DNLSE is defocusing and appropriate for vortices. If, instead, of small capacitances, oscillators are coupled by large inductances, then a focusing DNLSE arises. That case has been already studied previously (on uniform lattices) in the context of discrete solitons, breathers, and vortex solitons [55,56,60–62]. From a formal viewpoint, each inductor represents a separate degree of freedom. Therefore, our scheme is mathematically different. From a practical viewpoint, small capacitors on links are more convenient than large inductors.

It should be noted that electric networks can be of macroscopic sizes and assembled of standard radiotechnical elements. Typical dispersive and nonlinear times can be about milliseconds with the carrier frequency $\omega_0/2\pi$ of order 1 MHz. Additional convenience of electric implementation is in easy setting the model parameters and in controllability including arbitrary variation of coupling capacitances with time. Moreover, flexible wires make possible to construct topologically nontrivial 2D discrete manifolds as Möbius strip, torus, Klein bottle, projective plane, and so on. This fact opens wide new perspectives in studying vortices on such discretized surfaces. Another important thing is that our electric scheme can be equally suitable for construction of 3D nonlinear lattices. A practical problem is only in a very big number of elements. So, to observe interesting nonlinear behavior of vortices, in a 2D lattice, we need about $\mathsf{N}_{2D} \sim 10^3$–$10^4$ individual oscillators, whereas, for a 3D lattice, the required number is $\mathsf{N}_{3D} \sim 10^5$–$10^6$. Therefore, planar constructions seem more realistic at the moment.

Since the electric model is very promising, we put also the second goal in this paper, that is to simulate the dynamics directly within equations of motion governing the scheme in Fig. 1 and then compare the results with the DNLSE simulations.

This article is organized as follows. In Sec. II, we introduce the theoretical model and derive the corresponding DNLSE together with the parameters. Some technical details about the DNLSE are included because it is easier for theoretical analysis than the basic system of circuit equations. In Sec. III, we generally analyze vortex motion in the 2D case with orientation on the quasicontinuous limit. Special attention is given there to coupling profiles with a barrier. This feature is new in comparison with Ref. [25]. In Sec. IV, we present some numerical results demonstrating nontrivial behavior of interacting vortices in discrete spatially nonuniform weakly dissipative 2D systems. Both the DNLSE and the original system of circuit equations are simulated. In particular, it will be shown that depending on parameters, vortex clusters can be stably trapped for some initial period of time by a circular barrier in function $f$ profile, but then, due to gradual dissipative broadening of vortex cores, they lose stability and suddenly start to move in a complicated manner, some of vortices penetrating the barrier. Finally, Sec. V contains a brief summary of the paper.

## II. MODEL DESCRIPTION AND BASIC EQUATIONS

In the beginning, we describe our simple scheme (see Fig. 1). Let each electric oscillator in the network consist of a coil with inductance $L$ and small active resistance $R_L$, connected in series to a voltage-dependent differential capacitance (varicap) $C_v(V) = dq/dV$, where $q$ is the electric charge. A reverse-biased varactor diode is implied or another nonlinear capacitor (perhaps in parallel with an ordinary capacitor). The varicap is characterized by a large shunt resistance $R_C$ (for leakage current). For simplicity, we assume $R_C = \text{const}$, thus, neglecting nonlinearity in dissipation. The remaining end of the coil is connected to a dc bias voltage $V_b$, whereas the remaining contact of the varicap is grounded. A voltage at the contact between the coil and the varicap is $V_b + V_n(t)$. Functional dependencies $C(V_n) = C_v(V_b + V_n)$ differ for devices fabricated under different technologies, so many expressions were suggested to approximate them. In particular, for a reverse-biased diode in parallel with a constant capacitor, the following combined formula is able to ensure good accuracy within a sufficiently wide voltage range

(see, e.g., Refs. [51,53,56,60,61]),

$$C(V_n) = C_0\left[\mu + \frac{(1-\mu)}{(1+V_n/V_*)^\nu} + \eta e^{-\kappa V_n}\right]\Big/(1+\eta), \quad (5)$$

with fitting parameters $C_0 = C(0)$, $V_*$, $\mu$, $\nu$, $\eta$, and $\kappa$. Here, $0 < \mu < 1$ takes into account an ordinary capacitor in parallel, whereas $0.3 \lesssim \nu \lesssim 6.0$ is related to the diode (by the way, for the Toda lattice implementation, one needs to take diodes with $\nu = 1$). Very often in theoretical studies, it is put $\eta = 0$. In some research works, a different kind of variable capacitor is also considered with $C(V_n) = C_0(1 + V_n^2/V_*^2)$ [63]. Such a symmetric dependence is possible in devices using special nonlinear dielectric films [65]. In any case, (additional) accumulated electrostatic energy at the varicap is given by formula,

$$W(V_n) = \int_0^{V_n} C(u)u\,du, \quad (6)$$

whereas, the ac electric charge is

$$q_n = q(V_n) = \int_0^{V_n} C(u)du. \quad (7)$$

Taking the inverse relation, we have $V_n = U(q_n)$. The equation of motion for a single oscillator circuit with dissipative terms neglected is $L\ddot{q}_n + U(q_n) = 0$. It will be important for our purposes that a nonlinear frequency shift can be negative in this dynamics. Of course, the fully nonlinear regime should be studied numerically, but analytical investigations may be based on the expansion,

$$U(q_n) = C_0^{-1}\left[q_n + \alpha q_n^2 + \beta q_n^3 + \cdots\right] \quad (8)$$

assuming relatively small amplitudes. Then, a frequency shift for the weakly nonlinear regime is known to be

$$\Delta\omega = \omega_0(3\beta/8 - 5\alpha^2/12)q_0^2, \quad (9)$$

with $\omega_0 = 2\pi/T_0 = 1/\sqrt{LC_0}$ and $q_0$ being an amplitude of the main harmonics.

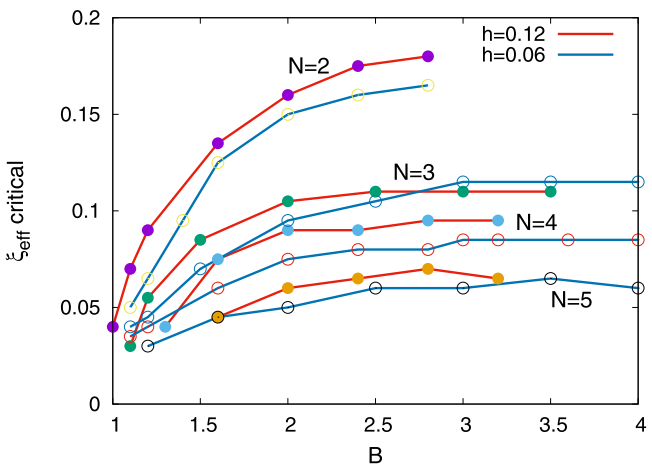


FIG. 2. Critical values of $\xi_{\text{eff}}$ found numerically by minimizing the Hamiltonian (36), starting with a small $\xi_{\text{eff}}$ and increasing it by small steps until cluster destruction.

The inverse quality factor of the oscillator is apparently,

$$\gamma = \left(R_L\sqrt{C_0/L} + R_C^{-1}\sqrt{L/C_0}\right)/2. \quad (10)$$

It is presumed very small (as we will see below, the most interesting things happening with vortices begin at $Q \gtrsim 10^4$). For example, with $L = 5.0 \times 10^{-4}H$, $C_0 = 5.0 \times 10^{-10}$ $F$, $R_L < 0.1$, and $R_C > 10^7$ $\Omega$, we have $\omega_0 = 2.0 \times 10^6$ rad/s, corresponding to a frequency about 0.3 MHz and a sufficiently high quality factor of $Q > 10^4$. Perhaps, even smaller values of $R_L$ and larger values of $R_C$ can be achieved at reasonably low temperatures, making $Q \gtrsim 10^5$.

There are also weak ordinary capacitors $C_{n,n'} \ll C_0$ inserted between points $V_n$ and $V_{n'}$. They unite individual oscillators into a whole network.

Equations of motion for the united system can be derived in a very simple manner. Indeed, electric current through the coil is $I_n$, whereas currents through the capacitors are $C(V_n)\dot{V}_n$ and $C_{n,n'}(\dot{V}_n - \dot{V}_{n'})$. The leakage current parallel to varicap is $V_n/R_C$. Thus, we obtain equations,

$$C(V_n)\dot{V}_n + \sum_{n'} C_{n,n'}(\dot{V}_n - \dot{V}_{n'}) + \frac{V_n}{R_C} = I_n. \quad (11)$$

A voltage difference at the coil is $L\dot{I}_n + R_L I_n$. In sum with $V_b + V_n$, it should give $V_b$. Therefore, we have the second subset of equations, closing the system,

$$L\dot{I}_n + V_n + R_L I_n = 0. \quad (12)$$

It is clear that our system admits a class of $n$-independent solutions related to Eq. (3) when each node oscillates as if there were no couplings.

It is not so obvious at first glance but can be easily checked that, without dissipative terms containing active resistances $R_L$ and $R_C$, Eqs. (11) and (12) correspond to a Lagrangian system with the Lagrangian function,

$$\mathsf{L} = \sum_n \frac{L}{2}\left[C(V_n)\dot{V}_n + \sum_{n'} C_{n,n'}(\dot{V}_n - \dot{V}_{n'})\right]^2 - \sum_n W(V_n) - \sum_{n,n'} \frac{C_{n,n'}}{4}(V_n - V_{n'})^2. \quad (13)$$

Equations of motion in the form (11) and (12) are suitable enough for numerical simulations but difficult for theoretical analysis. Therefore, our next steps will be to rewrite the Lagrangian in terms of charges $q_n$ and then introduce a Hamiltonian description. It is convenient to adopt nondimensionalization (voltage in units of $V_*$, charge in units of $C_0V_*$, and time in units of $1/\omega_0$), formally corresponding to $L = 1$, $C_0 = 1$. Then, in the first order on small quantities $\bar{c}_{n,n'} = C_{n,n'}/C_0$, and retaining only main terms on oscillation amplitudes in the couplings, we have

$$\mathsf{L} \approx \sum_n \left[\frac{\dot{q}_n^2}{2} - \frac{q_n^2}{2} - \alpha\frac{q_n^3}{3} - \beta\frac{q_n^4}{4}\right] + \frac{1}{4}\sum_{n,n'} \bar{c}_{n,n'}[2(\dot{q}_n - \dot{q}_{n'})^2 - (q_n - q_{n'})^2]. \quad (14)$$

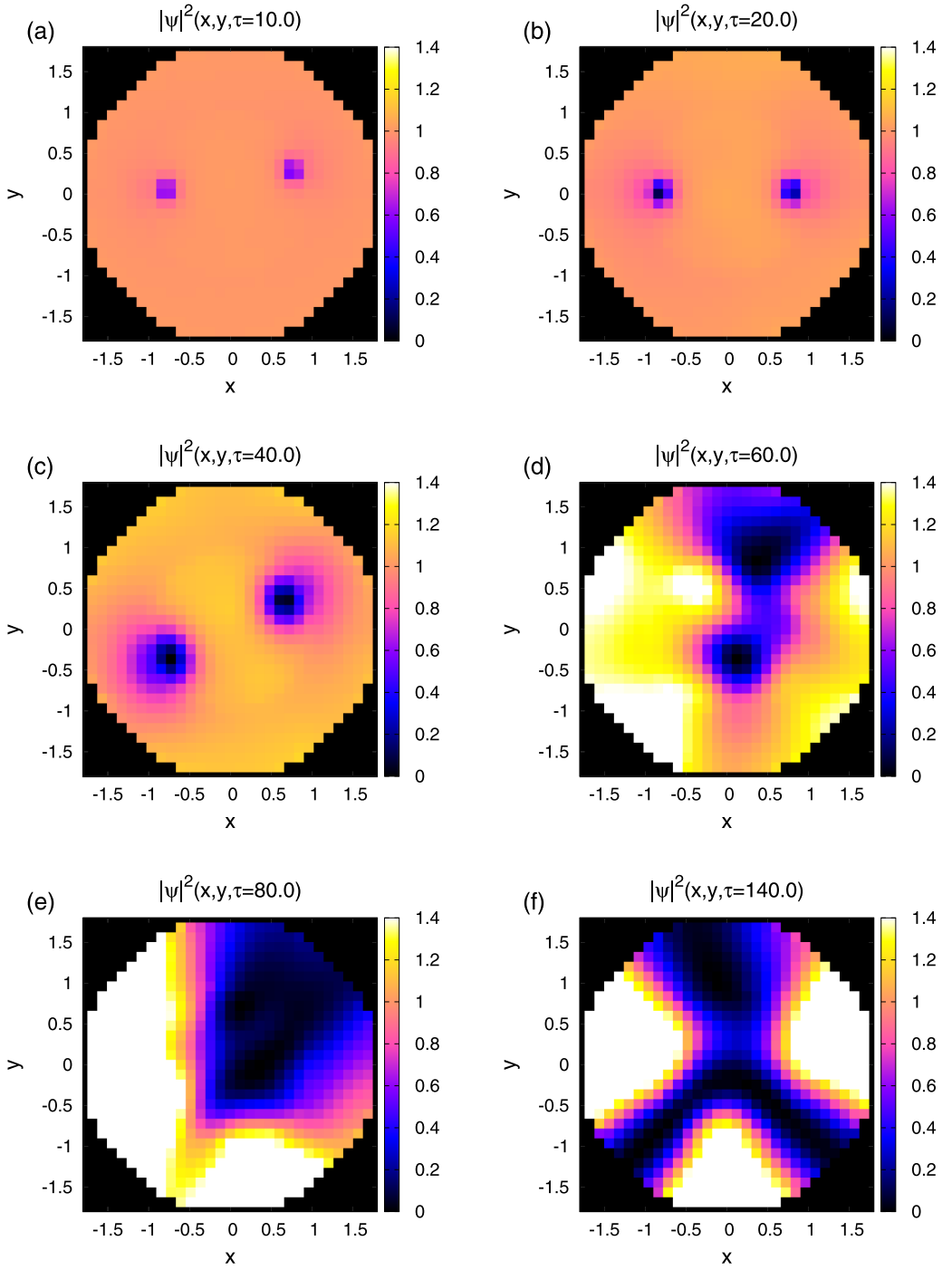


FIG. 3. An example of the evolution of two vortices in the DNLSE.

The canonical momenta for this Lagrangian are

$$p_n = \dot{q}_n + 2\sum_{n,n'} \bar{c}_{n,n'}(\dot{q}_n - \dot{q}_{n'}). \tag{15}$$

Inverse relations, again, with the first-order accuracy on $\bar{c}_{n,n'}$, are easily obtained as

$$\dot{q}_n \approx p_n - 2\sum_{n,n'} \bar{c}_{n,n'}(p_n - p_{n'}). \tag{16}$$

As the result, the Hamiltonian function of weakly interacting oscillators acquires the following form:

$$\mathsf{H} \approx \sum_n \left[\frac{p_n^2}{2} + \frac{q_n^2}{2} + \alpha\frac{q_n^3}{3} + \beta\frac{q_n^4}{4}\right] - \frac{1}{4}\sum_{n,n'} \bar{c}_{n,n'}[2(p_n - p_{n'})^2 - (q_n - q_{n'})^2]. \tag{17}$$

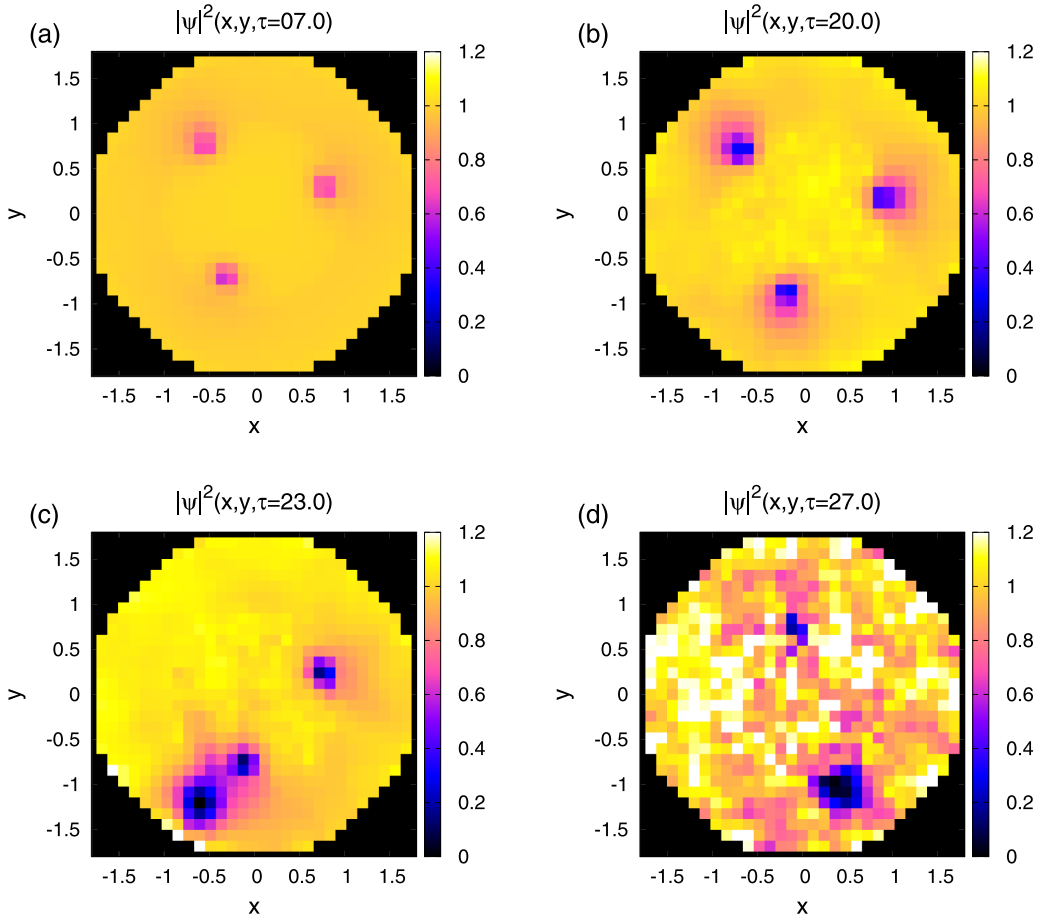


FIG. 4. An example of the evolution of three vortices in the DNLSE.

When an oscillator is taken separately, then, there exists a weakly nonlinear canonical transform,

$$q_n \approx \tilde{q}_n - \frac{\alpha}{3}(\tilde{q}_n^2 + 2\tilde{p}_n^2) + \frac{\tilde{q}_n}{16}\left[\left(\frac{25}{9}\alpha^2 - \frac{5}{2}\beta\right)\tilde{q}_n^2 + \left(\frac{13}{9}\alpha^2 - \frac{9}{2}\beta\right)\tilde{p}_n^2\right], \tag{18}$$

$$p_n \approx \tilde{p}_n + \frac{2\alpha}{3}\tilde{p}_n\tilde{q}_n - \frac{\tilde{p}_n}{16}\left[\left(\frac{11}{9}\alpha^2 - \frac{15}{2}\beta\right)\tilde{q}_n^2 + \left(\frac{47}{9}\alpha^2 - \frac{3}{2}\beta\right)\tilde{p}_n^2\right], \tag{19}$$

such that a combination $a_n = (\tilde{q}_n + i\tilde{p}_n)/\sqrt{2}$ (the normal complex variable) is related to the action-angle variables $S_n$ and $\phi_n$ by formula $a_n = \sqrt{S_n}\exp(i\phi_n)$. That transform excludes third-order terms from the partial Hamiltonians. Neglecting again nonlinearities in the couplings, we reduce the total Hamiltonian to the following expression:

$$\begin{aligned} \mathsf{H} \approx & \sum_n \left(|a_n|^2 + \frac{g}{2}|a_n|^4\right) \\ & -\frac{1}{4}\sum_{n,n'} \bar{c}_{n,n'}(a_n - a_{n'})(a_n^* - a_{n'}^*) \\ & +\frac{3}{8}\sum_{n,n'} \bar{c}_{n,n'}[(a_n - a_{n'})^2 + (a_n^* - a_{n'}^*)^2], \end{aligned} \tag{20}$$

where the nonlinear coefficient is $g = (3\beta/4 - 5\alpha^2/6)$. In terms of $a_n$, Hamiltonian equations of motion are $i\dot{a}_n = \partial\mathsf{H}/\partial a_n^*$. In the main approximation, $a_n$ behaves proportionally to $\exp(-it)$ since the nonlinearity and the couplings are weak. Therefore, the last double sum in Eq. (20) contains quickly oscillating quantities which are not important after averaging. Introducing slow envelopes $A_n = a_n\exp(it)$ and taking into account linear damping (not covered by Hamiltonian theory), we arrive at Eq. (2) with negative $c_{n,n'} = -\bar{c}_{n,n'}$. Nonlinear coefficient $g$, for physically relevant parameters in Eq. (5), appears also negative. In particular, if $\eta = 0$, then

$$g = \frac{\nu(1-\mu)}{24}[-3 + \nu(1 - 4\mu)]. \tag{21}$$

It is very important that a nonzero value of $\mu$, corresponding to a constant capacitor in parallel with the diode, results in stronger negative frequency shift. For example, with $\nu = 2$ and $\mu = 0.5$, we have $g = -5/24$, whereas for $\nu = 2$ and $\mu = 0$, it is $g = -1/12$.

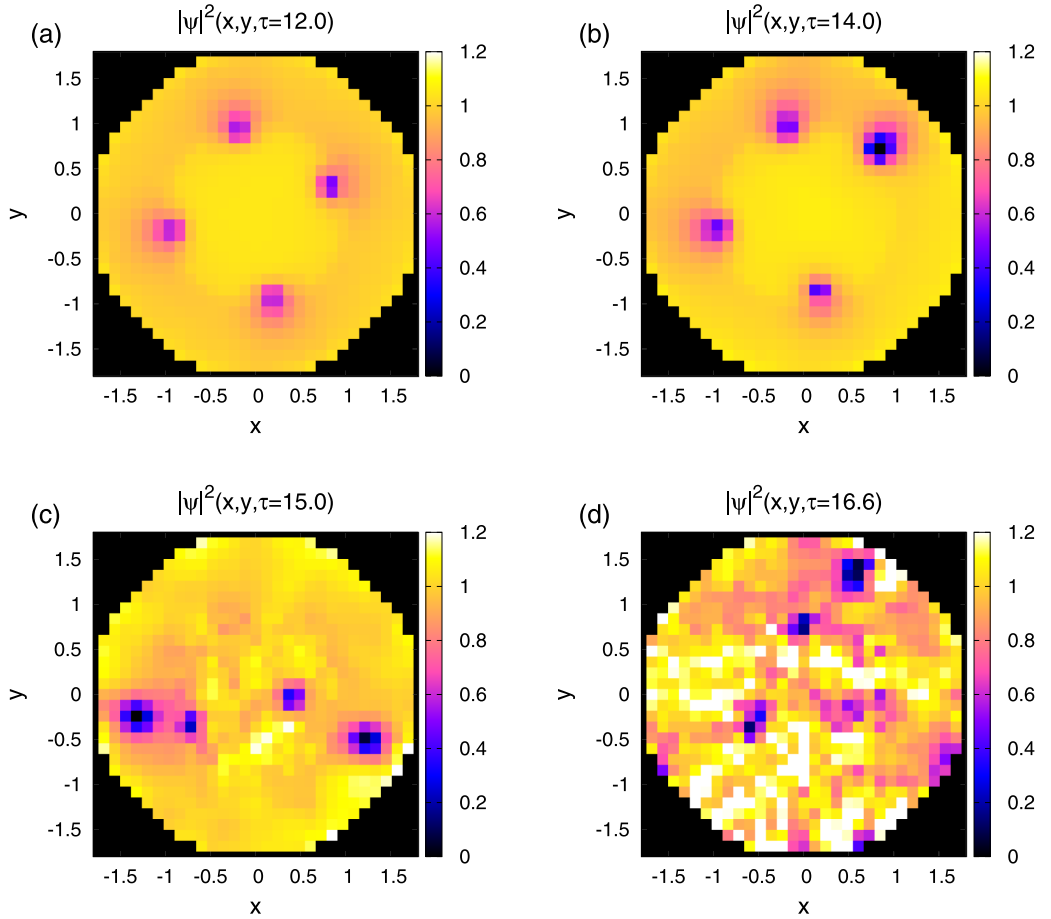


FIG. 5. An example of the evolution of four vortices in the DNLSE.

### III. ANALYSIS OF VORTEX MOTION IN 2D

As far as our goal is to study vortices on 2D networks, it is convenient to introduce new complex variables $\psi_n(t)$ through the following substitution (compare to Ref. [25] where a positive frequency shift was considered):

$$A_n(t) = A_0\psi_n^*(t)\exp[-\gamma t - i\varphi(t)], \tag{22}$$

where real $A_0$ is a typical amplitude at $t = 0$ and $\varphi(t) = gA_0^2(1 - e^{-2\gamma t})/(2\gamma)$. As the result, we reduce our dissipative autonomous system to a nonautonomous Hamiltonian system,

$$i\dot{\psi}_n = \sum_{n'} \frac{\bar{c}_{n,n'}}{2}(\psi_n - \psi_{n'}) + \left|gA_0^2\right|e^{-2\gamma t}(|\psi_n|^2 - 1)\psi_n. \tag{23}$$

Let a typical value of $\bar{c}_{n,n'}$ be $\bar{c} \ll 1$. For purposes of further analysis, we introduce a slow time $\tau = h^2\bar{c}t$ and small parameters,

$$\delta = \gamma/(h^2\bar{c}) \ll 1, \quad \xi = \left(h^2\bar{c}/\left|gA_0^2\right|\right)^{1/2} \ll 1. \tag{24}$$

Then, Eq. (23) takes the following form:

$$i\frac{d\psi_{\mathbf{n}}}{d\tau} = \sum_{\mathbf{n}'} \frac{F_{\mathbf{n},\mathbf{n}'}}{2h^2}(\psi_{\mathbf{n}} - \psi_{\mathbf{n}'}) + \frac{e^{-2\delta\tau}}{\xi^2}(|\psi_{\mathbf{n}}|^2 - 1)\psi_{\mathbf{n}}, \tag{25}$$

where $\mathbf{n}'$'s are the nearest neighbors for $\mathbf{n}$ on the square lattice, $F_{\mathbf{n},\mathbf{n}'} = F(h[\mathbf{n} + \mathbf{n}']/2)$, and $F(\mathbf{r}) \sim 1$ is a non-negative function. In the continuous limit, the above equation reduces to a defocusing NLSE with a spatially variable dispersion coefficient and a time-dependent nonlinear coefficient,

$$i\psi_\tau = -\frac{1}{2}\nabla\cdot[F(\mathbf{r})\nabla\psi] + \frac{e^{-2\delta\tau}}{\xi^2}(|\psi|^2 - 1)\psi. \tag{26}$$

We are interested in vortices on constant background $\psi_0 = 1$. It is clear from the equation above that intervals $\Delta\tau \sim 1$ are typical vortex turnover times in the system, $\xi$ is a typical relative healing length at $\tau = 0$, whereas,

$$\tilde{\xi}(\mathbf{r}, \tau) = \xi e^{\delta\tau}\sqrt{F(\mathbf{r})} \tag{27}$$

is a local relative vortex core width. Vortices described by Eq. (26) have been analyzed in Ref. [25] for the 3D case. Applying a similar analysis to the 2D situation, we easily obtain that coordinates $x_j$ and $y_j$ of $N$ point vortices are canonically conjugate quantities (up to vortex signs $\sigma_j = \pm 1$). On not very long times and for small $\xi$, when $\xi_{\text{eff}} = \xi\ \exp(\delta\tau) \ll 1$, vortex motion is approximately described by a time-dependent Hamiltonian function (compare to Refs. [40,41]),

$$H = \sum_j \sigma_j^2\mathcal{E}(\mathbf{r}_j, \tau) + {\sum_{j,k}}' \frac{\sigma_j\sigma_k}{2}G(\mathbf{r}_j, \mathbf{r}_k), \tag{28}$$

$$\mathcal{E}(\mathbf{r}, \tau) \approx \frac{1}{2}G[\mathbf{r} - \mathbf{e}\tilde{\xi}(\mathbf{r}, \tau)/2, \mathbf{r} + \mathbf{e}\tilde{\xi}(\mathbf{r}, \tau)/2], \tag{29}$$

where the prime means omitting diagonal terms in the double sum determining pair interactions between vortices, $\mathbf{e}$ is a

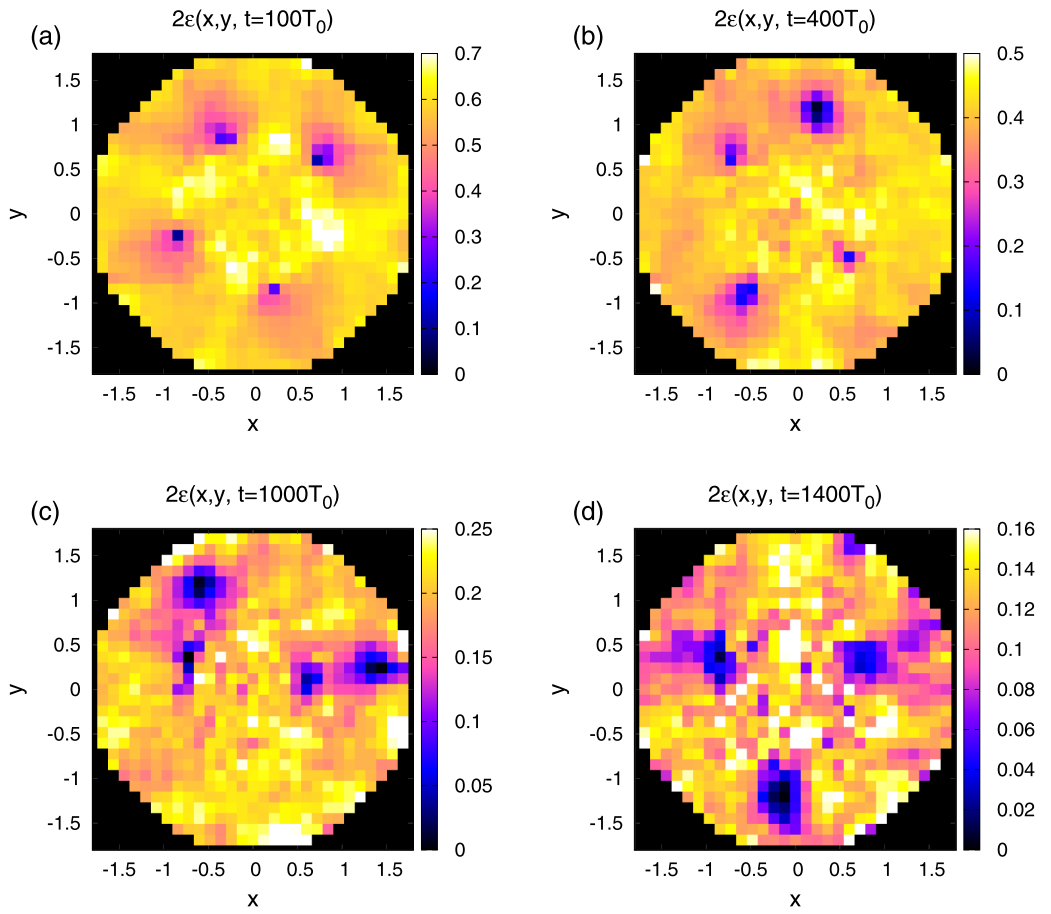


FIG. 6. An example of the evolution of four vortices in the basic electric model.

unit vector, and a two-dimensional Green's function $G(\mathbf{r}, \mathbf{r}_1)$ satisfies equation,

$$-\nabla_{\mathbf{r}} \cdot \frac{1}{F(\mathbf{r})} \nabla_{\mathbf{r}} G(\mathbf{r}, \mathbf{r}_1) = 2\pi \delta_{\text{Dirac}}(\mathbf{r} - \mathbf{r}_1). \tag{30}$$

The physical meaning of $G(\mathbf{r}, \mathbf{r}_1)$ can be explained as follows. Let $\psi = \sqrt{\rho} \exp(i\Phi)$ be the Madelung transform, and $\mathbf{J} = \rho F(\mathbf{r}) \nabla \Phi$ be a "current density" (in the hydrodynamic sense) for Eq. (26). In the long-scale hydrodynamic regime, away from vortex cores, we have $\rho \approx 1$ and, thus, $\nabla \cdot \mathbf{J} \approx 0$, so a stream function $\Theta$ exists for 2D vector field $F(\mathbf{r})\nabla\Phi$. Since the $\Phi$ field created by vortices is not single valued and has singularities, it satisfies equation $\text{curl}_{2D} \nabla \Phi = 2\pi \sum_j \sigma_j \delta_{\text{Dirac}}(\mathbf{r} - \mathbf{r}_j)$. Therefore, we have a partial differential equation determining the stream function,

$$-\nabla_{\mathbf{r}} \cdot \frac{1}{F(\mathbf{r})} \nabla_{\mathbf{r}} \Theta(\mathbf{r}) = 2\pi \sum_j \sigma_j \delta_{\text{Dirac}}(\mathbf{r} - \mathbf{r}_j). \tag{31}$$

So $G(\mathbf{r}, \mathbf{r}_1)$ is a stream function created at point $\mathbf{r}$ by a vortex placed in point $\mathbf{r}_1$. Expression (28) for vortex Hamiltonian $H$ then follows from appropriately regularized "kinetic-energy" integral:

$$2\pi H = \frac{1}{2} \int \frac{(\nabla \Theta)^2}{F(\mathbf{r})} d^2\mathbf{r}. \tag{32}$$

It follows from Eq. (30) that

$$G(\mathbf{r}_1, \mathbf{r}_2) = \tilde{\theta}(\mathbf{r}_1, \mathbf{r}_2) - \sqrt{F(\mathbf{r}_1) F(\mathbf{r}_2)} \ln |\mathbf{r}_1 - \mathbf{r}_2|, \tag{33}$$

with some smooth function $\tilde{\theta}(\mathbf{r}_1, \mathbf{r}_2) \sim 1$. Therefore, the self-energy is

$$\mathcal{E}(\mathbf{r}, \tau) = \theta(\mathbf{r}) - \frac{1}{2} F(\mathbf{r}) \{\ln[\xi \sqrt{F(\mathbf{r})}] + \delta\tau\}, \tag{34}$$

where $\theta(\mathbf{r}) = \tilde{\theta}(\mathbf{r}, \mathbf{r})/2$.

In particular, we may take the circularly symmetric profile $F(r)$ with $r = \sqrt{x^2 + y^2}$, and roughly (with a logarithmic accuracy) estimate energy of a vortex cluster in the form of a regular $N$ polygon,

$$E_N(r, \tau) \approx \frac{N}{2} F(r) [\Lambda(\tau) - (N-1) \ln(r)], \tag{35}$$

where $\Lambda(\tau) = [\ln(1/\xi) - \delta\tau] = -\ln(\xi_{\text{eff}})$ is a logarithmically large quantity. It is not difficult to understand that, if $F(r)$ has a barrier at some finite $r_b$, and $N$ is not too large, then expression (35) may have a minimum at some $0 < r_* < r_b$. Thus, whereas $\xi_{\text{eff}}$ is less than a critical value, such a profile is able to trap a vortex cluster.

Discreteness (finite $h$) acts also to stabilize vortex configurations because, whereas $\xi_{\text{eff}} \lesssim h$, the lattice tends to create local minima (in the internode vortex center positions) for the

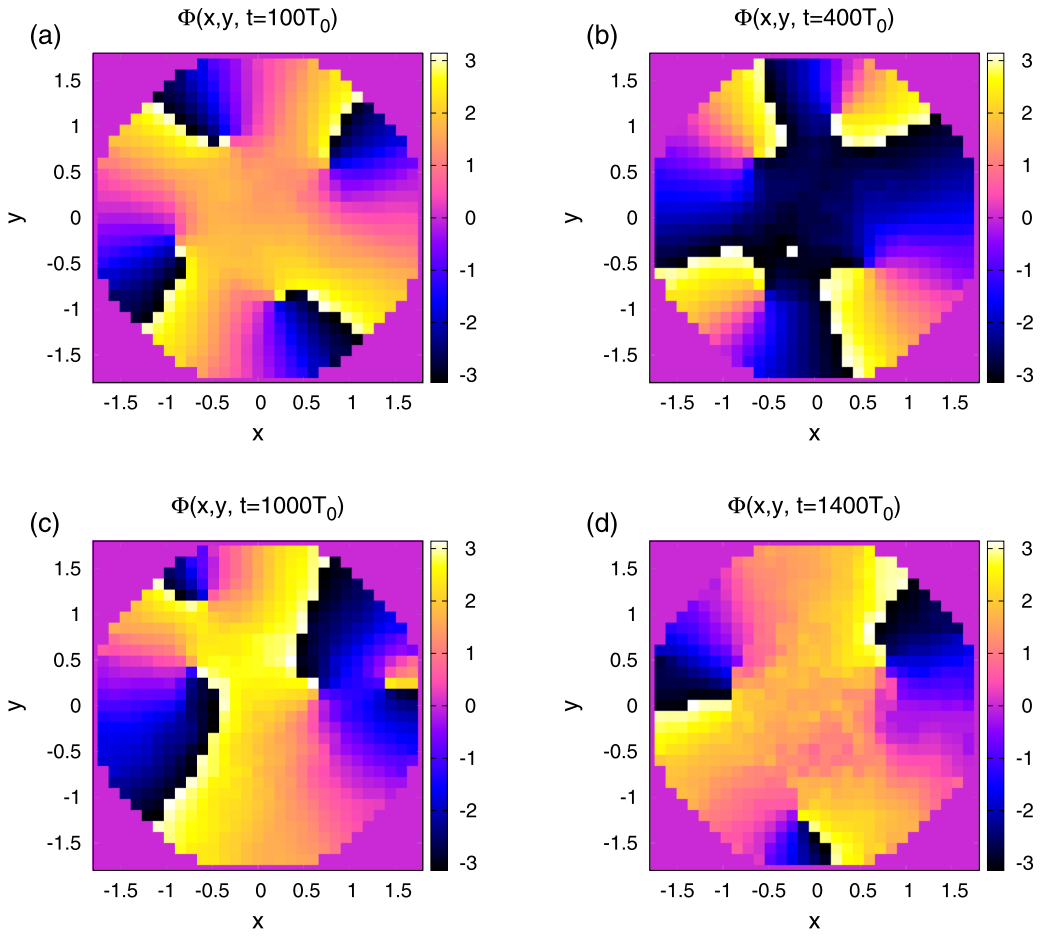


FIG. 7. Four vortices in the electric model: phases corresponding to Fig. 6. The presence of vortices is clearly seen.

Hamiltonian corresponding to Eq. (25),

$$\tilde{\mathsf{H}} = \sum_{\mathbf{n},\mathbf{n}'} \frac{F_{\mathbf{n},\mathbf{n}'}}{4h^2} |\psi_{\mathbf{n}} - \psi_{\mathbf{n}'}|^2 + \sum_{\mathbf{n}} \frac{e^{-2\delta\tau}}{2\xi^2} (|\psi_{\mathbf{n}}|^2 - 1)^2. \quad (36)$$

Figure 2 illustrates this fact for a particular case of "rectangular" barrier [$F(r) = 1$ if $r^2 < 1$, and $F(r) = B > 1$ if $1 \leqslant r^2 < 3$; otherwise $F = 0$]. There, for different $N$'s, and for two different values of $h$, numerical estimates are presented how the critical value of parameter $\xi_{\text{eff}}$ depends on barrier height $B$. It is seen that spatial nonuniformity of the links has a strong influence on vortex stability for $1 \lesssim B \lesssim 3$. However, saturation on larger $B$ is still waiting for an explanation.

So we can expect stable trapping of a few vortices of the same sign within a domain surrounded by the barrier. However, as time increases, function $\Lambda(\tau)$ decreases, and, therefore, vortex configuration should suddenly become unstable at some moment. In the next section, we numerically verify such a scenario within Eq. (25) and, then, within Eqs. (11) and (12).

## IV. NUMERICAL RESULTS

Equation (25) has been numerically simulated using a fourth-order Runge-Kutta scheme for time stepping. Function $F(r)$ was taken in the above described simple form with $B = 3.0$. That corresponds to using just two kinds of coupling capacitors $C_{n,n'}$. Thus, we have a compact planar structure with a finite number of interacting degrees of freedom.

We present numerical results for $N = 2$, $N = 3$, and $N = 4$ vortices (Figs. 3–5, respectively, where each vortex is seen as a density depletion). The parameters in these numerical experiments were as follows: $h = 0.12$, $\xi = 0.05$, and $\delta = 0.04$. As initial states, we took nonsymmetric vortex configurations corresponding to numerically found local minima of Hamiltonian (36).

The most regular dynamics was observed for $N = 2$, perhaps, because the simplified continuous counterpart (28) is an integrable system in the case of two vortices (besides the Hamiltonian, the angular momentum is conserved). After the initial quasistatic period of evolution [Fig. 3(a)], there was stage of oscillatory motion without orbiting [Fig. 3(b)]. Then, it was orbiting in anticlockwise azimuthal direction with gradually widening cores [Figs. 3(c) and 3(d)]. Finally, wide vortices comparable to the whole system size were transformed to a wave structure propagating mainly clockwise [Figs. 3(e) and 3(f)]. The last stage was practically in a linear regime because the effective nonlinear coefficient $\exp(-2\delta\tau)/\xi^2$ was very small at $\tau \gtrsim 100$.

Vortex clusters with $3 \leqslant N \leqslant 5$ passed similar initial two stages in their evolution, but the, subsequent, dynamics was different. The first stage was again a stable nearly static configuration when vortex centers were motionless whereas their

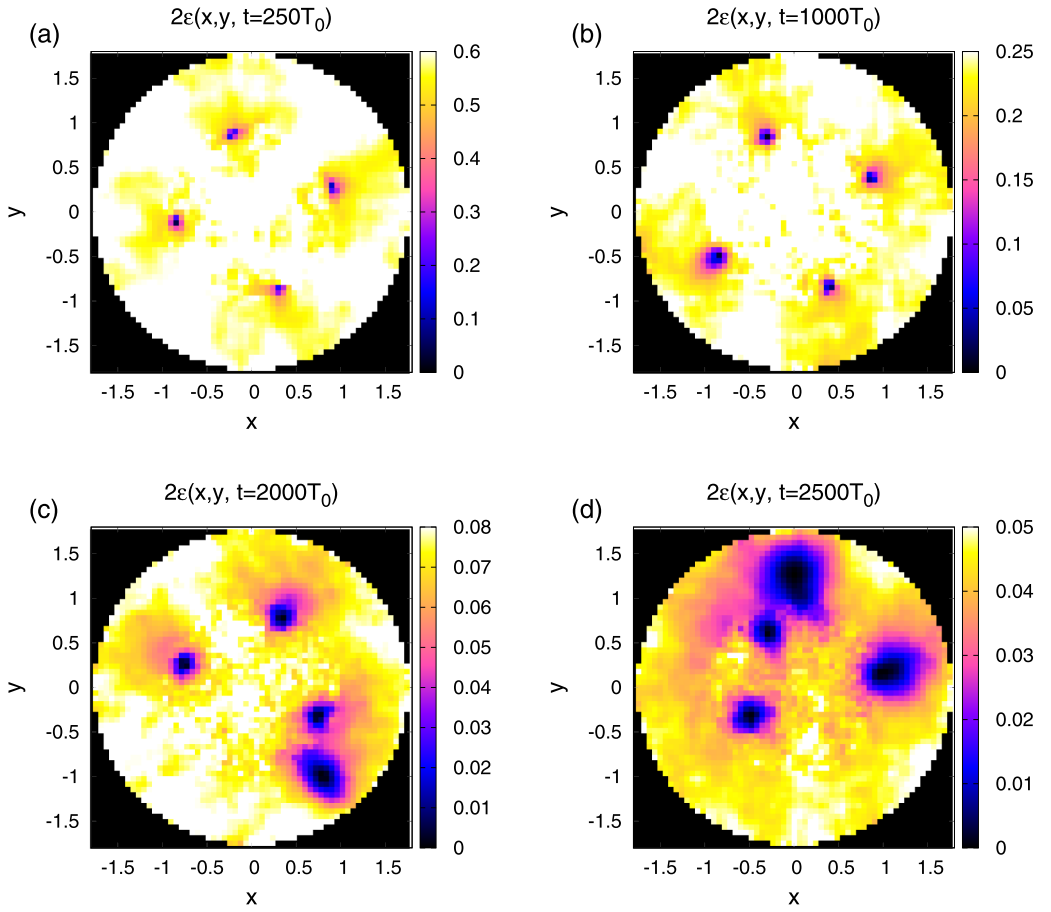


FIG. 8. An example of the evolution of four vortices in the electric model with smaller $h = 0.06$.

cores gradually broadened according to Eq. (27) [Figs. 4(a) and 5(a)]. The second stage was the oscillation of vortices around their previous positions [Figs. 4(b) and 5(b)]. At the third stage, vortices lose stability and begin to move in a complicated manner, typically, one or two of them at fast external orbits [Figs. 4(c) and 5(c)]. At the fourth stage, the external vortices quit the lattice producing strong short-scale nonvortical oscillations in it [Figs. 4(d) and 5(d)]. During a further evolution, some of the remaining vortices go to external orbits and leave the lattice in a similar manner until one or two are present on a highly disturbed background (not shown).

Static initial configurations with $N \geqslant 6$ were not found with the given parameters. However, cases $N = 6$ and $N = 6 + 1$ (hexagon plus central vortex) were successfully simulated with $h = 0.04$, $\xi = 0.025$, and $\delta = 0.02$ (not shown). It should be noted that, for this case, the quality factor should be extremely high since $\gamma/gA_0^2 = \delta\xi^2 \sim 10^{-5}$, whereas $gA_0^2 \sim 0.1$. The dynamics was qualitatively similar to that described above. It is interesting to note that, in the last case, the central vortex lost stability first and quickly passed to external orbit, crossing the system boundary soon after that.

Of course, the above results were obtained within the DNLSE under many simplifying assumptions, and, therefore, they cannot be completely convincing. In order to get more direct evidence of vortex existence and behavior in fully nonlinear regime, the original system of circuit equations (11) and (12) has been numerically simulated using expression (5) with parameters $\eta = 0$, $\nu = 2$, $\mu = 0.5$ (and $C_0 = 1$, $V_* = 1$). Two numerical experiments are presented below. In the first one (see Figs. 6 and 7), the remaining dimensionless parameters were $\bar{c} = 0.02$, $h = 0.12$, $L = 1$, $R_L = 10^{-4}$, $R_C = 10^4$. At $t = 0$, the partial energies of oscillators were corresponding to $I_n^2/2 + W(V_n) = 0.32$ (excluding vortex cores), whereas their phases $\Phi_n = \arctan(I_n/V_n)$ were the same as the initial phases for the DNLSE simulation. Therefore, $|gA_0^2| \approx (5/24)0.32 \approx 0.067$ in these numerical experiments. Initial ac voltages were in the range of $-0.6 \lesssim V_n \lesssim 1.0$.

To resolve Eqs. (11) with respect to $\dot{V}_n$, a simple iterative scheme was developed,

$$D_n^{(j+1)} = D_n^{(j)} - 0.2\Big[C(V_n)D_n^{(j)} + \sum_{n'} C_{n,n'}\big(D_n^{(j)} - D_{n'}^{(j)}\big) + \frac{V_n}{R_C} - I_n\Big], \tag{37}$$

with $D_n^{(0)} = (I_n - V_n/R_C)/C(V_n)$. The result of the 60th iteration $\dot{V}_n \approx D_n^{(60)}$ was then used in a Runge-Kutta fourth-order time stepping. The convergence of this scheme was ensured by positive definiteness of the corresponding quadratic form and by choosing the coefficient 0.2 sufficiently small to have $|1 - 0.2C_{\max}| < 1$ [where $C_{\max} = C(V_{\min})$, and $V_{\min} \approx -0.57$ is the negative root of equation $W(V) = 0.32$].

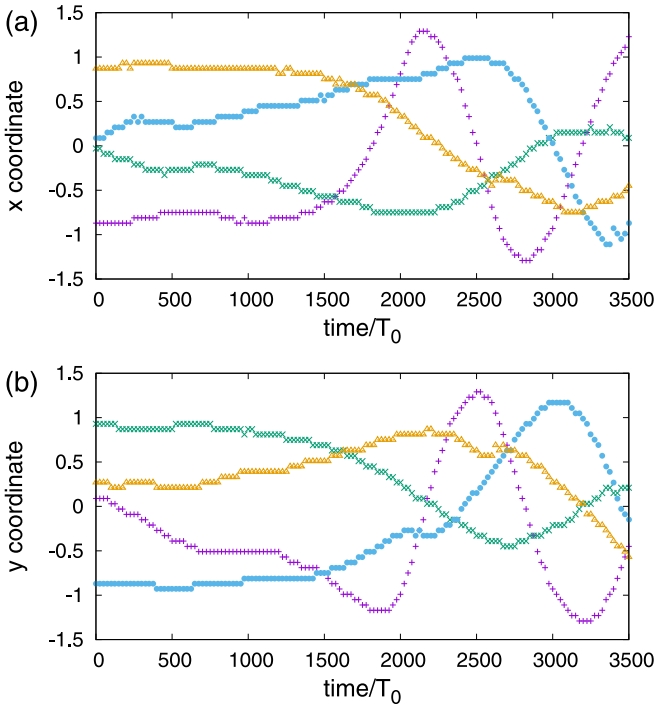


FIG. 9. Time dependence of $x$ and $y$ coordinates of four vortices, corresponding to simulation with $h = 0.06$. Conventionally, vortices are located at the centers of those $h \times h$ squares where the sum of phase increments along the sides is $2\pi$.

In Fig. 6, the evolution of quantities $2\varepsilon_n = I_n^2 + 2W(V_n)$ is shown for the case of four vortices, whereas, in Fig. 7, we see the corresponding phases. In particular, Fig. 7 indicates unambiguously that we deal with vortices not simply with some amplitude depressions. Qualitatively, the system passed the same stages as in the simplified DNLSE model. However, since here the initial phase distribution was not appropriately adjusted to strong nonlinearity, the first (trapping) stage was not so long as in experiment shown in Fig. 5.

Finally, in Figs. 8 and 9, we present results for a smaller $h = 0.06$ and for larger initial energies $I_n^2 + 2W(V_n) = 0.81$. In this simulation, $\bar{c} = 0.04$. In general, vortices look smoother here. As Figs. 8(a) and 8(b) demonstrate, and Fig. 9 confirms, the cluster was almost static until $t \sim 1000T_0$. After that time, the configuration was deformed by appeared instability, and the vortices started intense motion. Unlike the case of $h = 0.12$, here, no vortex exited the disk until the very end of the simulation.

## V. SUMMARY

To summarize, in this paper, a general scheme of an electric network has been suggested which can be approximately described by a weakly dissipative defocusing discrete nonlinear Schrödinger equation of a special kind where coupling terms are not translationally invariant but spatially uniform background solutions exist. Discrete vortices in such systems have been analyzed and then numerically simulated. Simulations have demonstrated qualitatively similar results within the DNLSE and within the original circuit equations.

Of crucial importance is the quality factor of oscillator circuits. Numerical experiments have shown that nontrivial behavior of vortices is observable with $Q \gtrsim 10^4$–$10^5$. In practice, such values could be achieved at sufficiently low temperatures when conductivity of metals as well as resistivity of dielectrics are both substantially higher than they are at room temperature.

The study above is apparently far from being exhaustive. This system seems deserving further through investigation especially in its highly nonlinear regimes and under external driving (driving signals can be easily introduced into electric network, resulting in many resonance phenomena, perhaps, similar in some sense to those reported in Ref. [22]). The author also hopes that experimentalists will be interested in conducting laboratory experiments inspired by the present theory.

[1] L. M. Pismen, *Vortices in Nonlinear Fields* (Clarendon, Oxford, 1999).
[2] C. J. Pethick and H. Smith, *Bose-Einstein Condensation in Dilute Gases* (Cambridge University Press, Cambridge, UK, 2002).
[3] L. P. Pitaevskii and S. Stringari, *Bose-Einstein Condensation* (Oxford University Press, Oxford, 2003).
[4] P. G. Kevrekidis, D. J. Frantzeskakis, and R. Carretero-González, *The Defocusing Nonlinear Schrödinger Equation: From Dark Solitons and Vortices to Vortex Rings* (SIAM, Philadelphia, 2015).
[5] A. A. Svidzinsky and A. L. Fetter, Phys. Rev. A **62**, 063617 (2000).
[6] A. L. Fetter and A. A. Svidzinsky, J. Phys.: Condens. Matter **13**, R135 (2001).
[7] A. L. Fetter, Rev. Mod. Phys. **81**, 647 (2009).
[8] P. G. Kevrekidis, R. Carretero-González, D. J. Frantzeskakis, and I. G. Kevrekidis, Mod. Phys. Lett. B **18**, 1481 (2004).
[9] B. A. Malomed and P. G. Kevrekidis, Phys. Rev. E **64**, 026601 (2001).
[10] P. G. Kevrekidis, B. A. Malomed, D. J. Frantzeskakis, and R. Carretero-Gonzalez, Phys. Rev. Lett. **93**, 080403 (2004).
[11] R. Carretero-Gonzalez, P. G. Kevrekidis, B. A. Malomed, and D. J. Frantzeskakis, Phys. Rev. Lett. **94**, 203901 (2005).
[12] P. G. Kevrekidis, D. J. Frantzeskakis, R. Carretero-Gonzalez, B. A. Malomed, and A. R. Bishop, Phys. Rev. E **72**, 046613 (2005).
[13] F. Lederer, G. I. Stegeman, D. N. Christodoulides, G. Assanto, M. Segev, and Ya. Silberberg, Phys. Rep. **463**, 1 (2008).
[14] J. Cuevas, G. James, P. G. Kevrekidis, and K. J. H. Law, Physica D **238**, 1422 (2009).

[15] Ya. V. Kartashov, B. A. Malomed, and L. Torner, Rev. Mod. Phys. **83**, 247 (2011).
[16] M. Lapine, I. V. Shadrivov, and Yu. S. Kivshar, Rev. Mod. Phys. **86**, 1093 (2014).
[17] D. Hennig and G. P. Tsironis, Phys. Rep. **307**, 333 (1999).
[18] Yu. S. Kivshar and M. Peyrard, Phys. Rev. A **46**, 3198 (1992).
[19] S. V. Dmitriev, P. G. Kevrekidis, B. A. Malomed, and D. J. Frantzeskakis, Phys. Rev. E **68**, 056603 (2003).
[20] J.-K. Xue, A.-X. Zhang, and J. Liu, Phys. Rev. A **77**, 013602 (2008).
[21] G. Assanto, L. A. Cisneros, A. A. Minzoni, B. D. Skuse, N. F. Smyth, and A. L. Worthy, Phys. Rev. Lett. **104**, 053903 (2010).
[22] N. N. Rosanov, N. V. Vysotina, A. N. Shatsev, A. S. Desyatnikov, and Yu. S. Kivshar, Phys. Rev. Lett. **108**, 133902 (2012).
[23] M. J. Ablowitz, C. W. Curtis, and Y.-P. Ma, Phys. Rev. A **90**, 023813 (2014).
[24] M. J. Ablowitz and J. T. Cole, Phys. Rev. A **99**, 033821 (2019).
[25] V. P. Ruban, Phys. Rev. E **100**, 012205 (2019).
[26] B. Y. Rubinstein and L. M. Pismen, Physica D **78**, 1 (1994).
[27] V. P. Ruban, Phys. Rev. E **64**, 036305 (2001).
[28] A. Aftalion and T. Riviere, Phys. Rev. A **64**, 043611 (2001).
[29] J. J. Garcia-Ripoll and V. M. Pérez-García, Phys. Rev. A **64**, 053611 (2001).
[30] J. R. Anglin, Phys. Rev. A **65**, 063611 (2002).
[31] A. Aftalion and R. L. Jerrard, Phys. Rev. A **66**, 023611 (2002).
[32] P. Rosenbusch, V. Bretin, and J. Dalibard, Phys. Rev. Lett. **89**, 200403 (2002).
[33] A. Aftalion and I. Danaila, Phys. Rev. A **68**, 023603 (2003).
[34] A. Aftalion and I. Danaila, Phys. Rev. A **69**, 033608 (2004).
[35] I. Danaila, Phys. Rev. A **72**, 013605 (2005).
[36] A. L. Fetter, Phys. Rev. A **69**, 043617 (2004).
[37] T.-L. Horng, S.-C. Gou, and T.-C. Lin, Phys. Rev. A **74**, 041603(R) (2006).
[38] S. Serafini, M. Barbiero, M. Debortoli, S. Donadello, F. Larcher, F. Dalfovo, G. Lamporesi, and G. Ferrari, Phys. Rev. Lett. **115**, 170402 (2015).
[39] R. N. Bisset, W. Wang, C. Ticknor, R. Carretero-Gonzalez, D. J. Frantzeskakis, L. A. Collins, and P. G. Kevrekidis, Phys. Rev. A **92**, 063611 (2015).
[40] V. P. Ruban, JETP Lett. **105**, 458 (2017).
[41] V. P. Ruban, JETP **124**, 932 (2017).
[42] V. P. Ruban, JETP Lett. **106**, 223 (2017).
[43] V. P. Ruban, JETP **126**, 397 (2018).
[44] V. P. Ruban, JETP Lett. **108**, 605 (2018).
[45] S. Serafini, L. Galantucci, E. Iseni, T. Bienaime, R. N. Bisset, C. F. Barenghi, F. Dalfovo, G. Lamporesi, and G. Ferrari, Phys. Rev. X **7**, 021031 (2017).
[46] R. N. Bisset, S. Serafini, E. Iseni, M. Barbiero, T. Bienaime, G. Lamporesi, G. Ferrari, and F. Dalfovo, Phys. Rev. A **96**, 053605 (2017).
[47] W. Wang, R. N. Bisset, C. Ticknor, R. Carretero-Gonzalez, D. J. Frantzeskakis, L. A. Collins, and P. G. Kevrekidis, Phys. Rev. A **95**, 043638 (2017).
[48] C. Ticknor, W. Wang, and P. G. Kevrekidis, Phys. Rev. A **98**, 033609 (2018).
[49] C. Ticknor, V. P. Ruban, and P. G. Kevrekidis, Phys. Rev. A **99**, 063604 (2019).
[50] R. Hirota and K. Suzuki, J. Phys. Soc. Jpn. **28**, 1366 (1970); Proc. IEEE **61**, 1483 (1973).
[51] A. C. Hicks, A. K. Common, and M. I. Sobhy, Physica D **95**, 167 (1996).
[52] A. C. Singer and A. V. Oppenheim, Int. J. Bifurcation Chaos Appl. Sci. Eng. **9**, 571 (1999).
[53] D. Cai, N. Gronbech-Jensen, A. R. Bishop, A. T. Findikoglu, and D. Reagor, Physica D **123**, 291 (1998).
[54] T. Kofane, B. Michaux, and M. Remoissenet, J. Phys. C: Solid State Phys. **21**, 1395 (1988).
[55] P. Marquie, J. M. Bilbault, and M. Remoissenet, Phys. Rev. E **49**, 828 (1994).
[56] P. Marquie, J. M. Bilbault, and M. Remoissenet, Phys. Rev. E **51**, 6127 (1995).
[57] J. Leon and M. Manna, Phys. Rev. Lett. **83**, 2324 (1999).
[58] V. A. Makarov, E. del Rio, W. Ebeling, and M. G. Velarde, Phys. Rev. E **64**, 036601 (2001).
[59] D. Yemele, P. Marquie, and J. M. Bilbault, Phys. Rev. E **68**, 016605 (2003).
[60] L. Q. English, F. Palmero, A. J. Sievers, P. G. Kevrekidis, and D. H. Barnak, Phys. Rev. E **81**, 046605 (2010).
[61] F. Palmero, L. Q. English, J. Cuevas, R. Carretero-Gonzalez, and P. G. Kevrekidis, Phys. Rev. E **84**, 026605 (2011).
[62] L. Q. English, F. Palmero, J. F. Stormes, J. Cuevas, R. Carretero-Gonzalez, and P. G. Kevrekidis, Phys. Rev. E **88**, 022912 (2013).
[63] Y. Shen, P. G. Kevrekidis, G. P. Veldes, D. J. Frantzeskakis, D. DiMarzio, X. Lan, and V. Radisic, Phys. Rev. E **95**, 032223 (2017).
[64] F. Palmero, L. Q. English, X.-L. Chen, W. Li, J. Cuevas-Maraver, and P. G. Kevrekidis, Phys. Rev. E **99**, 032206 (2019).
[65] C. J. G. Meyers, C. R. Freeze, S. Stemmer, and R. A. York, Appl. Phys. Lett. **109**, 112902 (2016).